Initial Development and Verification of a Precise Orbit Determination Filter for the APEX CubeSat Mission

Kyle J. Craft, Grant R. Hecht

Undergraduate, Department of Mechanical and Aerospace Engineering, Missouri University of Science and Technology
400 West 13th Street, Rolla, MO 65409-0050
kczn6@mst.edu

Faculty Advisor: Henry J. Pernicka
Department of Mechanical and Aerospace Engineering, Missouri University of Science and Technology

ABSTRACT

Current research for the Advanced Propulsion Experiment (APEX) at Missouri University of Science and Technology is focused on precise orbit and parameter determination to verify the performance of the Multi-Mode Ionic Monopropellant thruster payload. A batch filter to process dual-frequency GPS pseudoranges using the International GNSS Service precise position, clock, and phase center data products was developed. The filter estimates the dynamic states of the vehicle in conjunction with the coefficients of drag and solar radiation pressure, a constant average thrust magnitude, and the time biases of the GNSS receiver clock at each measurement epoch. Furthermore, it considers uncertainty in the vehicle attitude and mass measurement. The framework is extended to support examination of other parameters of interest. The statistical consistency of the filter is verified using a Monte Carlo analysis. The filter dynamics and measurement models are verified using AGI's Systems Tool Kit and initial results of verification using NASA ICESat mission data are presented.

INTRODUCTION

The on-orbit performance and thrust determination of an experimental multi-mode CubeSat propulsion system is the primary objective of the Advanced Propulsion Experiment (APEX) mission being developed by Missouri University of Science and Technology (Missouri S&T) Satellite Research Team (M-SAT). The combination of a high-thrust, low-specific impulse catalytic chemical mode with a low-thrust, high-specific impulse electrospray mode makes the Multi-Mode Ionic Monopropellant Electrospray (MIME) thruster payload advantageous for a myriad of missions profiles, but presents a unique challenge in the on-orbit thrust determination component of the APEX mission. The low thrust produced in electrospray mode is undetectable by current accelerometers suitable for CubeSat missions. Low thrust is then typically detected by mounting the thruster such that an external torque is imparted on the satellite and the resulting attitude motion is used to indirectly determine thrust. However, the thrust created during chemical maneuvers, though detectable with an accelerometer, would produce an adversely high attitude rate on the vehicle. To prevent this, the thruster is placed such that the thrust vector line of action passes within close proximity of the center of mass (Figure 1). Therefore, the APEX mission then requires the development of a robust orbit determination algorithm capable of accurately estimating thrust from the resulting change in the orbit of the vehicle.

Previous M-SAT work has shown the feasibility and statistical consistency of processing GPS pseudoranges and star tracker data in a batch filter framework to determine the on-orbit thrust[1] as well as aid in APEX concept of operations development by examining maneuver architectures.[1,2] These results determined a maneuver applied normal to the orbit plane results in the most accurate thrust determination.
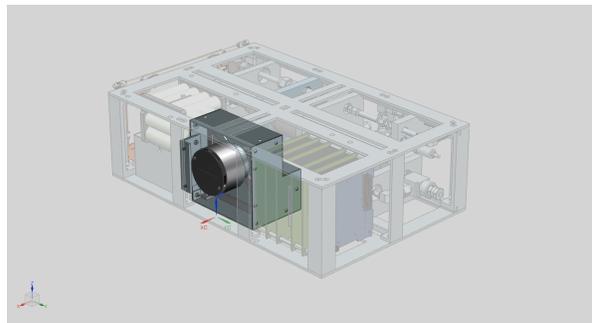

Figure 1: APEX CAD Model

Though previous work has shown promise with a batch filter scheme, additional considerations for the true on-orbit environment including errors in spacecraft mass, attitude, thrust vector misalignment, and corrections for atmospheric effects of GPS pseudoranges are required to ensure the filter will perform correctly with flight data. To address these issues, a consider batch filter framework

was incorporated to include the effect of uncertainties in the mass and attitude of APEX. A first order correction for ionospheric errors in GPS pseudoranges was also implemented. The statistical consistency and robustness of the new consider batch filter was tested using AGI's Systems Tool Kit (STK) and a Monte Carlo analysis. Finally, pseudorange data taken from the NASA ICESat-1 mission were processed using the developed filter and the determined trajectory was compared to the published trajectory. The resulting product was a robust statistical orbit determination filter compatible with commonly available CubeSat sensors and capable of accurate thrust determination.

THRUST DETERMINATION FILTER

Consider Batch Filter

The consider batch filter is an extension of the batch filter framework that allows for the inclusion of additional random variables in the full state vector that are not desired to be estimated, but whose uncertainties are desired to be included in the determination of state uncertainty.[3] The filter is an iterative, unbiased, least-squares estimator that determines a correction to an initial state at each iteration such that[3]

$$(\boldsymbol{x}_0^*)_n = (\boldsymbol{x}_0^*)_{n-1} + (\delta\hat{\boldsymbol{x}}_0)_n \tag{1}$$

where $(\boldsymbol{x}_0^*)_n$ represents the determined initial state at iteration n of the filter and $\delta\hat{\boldsymbol{x}}_n$ is the estimated correction to the initial state. The asterisk superscript, $(\cdot)^*$, denotes a quantity evaluated along the nominal trajectory and the caret notation, $(\hat{\cdot})$, denotes an estimated quantity.

For the inclusion of consider parameters, first, a concatenated full system state vector, $\mathbf{x}$, is defined at time t_k as

$$\mathbf{x}_k = \begin{bmatrix} \boldsymbol{x}_k^T & \boldsymbol{c}_k^T \end{bmatrix}^T \tag{2}$$

$$\boldsymbol{x}_k = \begin{bmatrix} \boldsymbol{r}_k^T & \dot{\boldsymbol{r}}_k^T & c_D & c_R & T & \Delta t_0 & \dots & \Delta t_l \end{bmatrix}^T \tag{3}$$

$$\boldsymbol{c}_k = \begin{bmatrix} \boldsymbol{q}_k & m \end{bmatrix}^T \tag{4}$$

where $\boldsymbol{x}$ contains the estimated/nominal states (hereafter referred to simply as the state), and $\boldsymbol{c}$ is the vector containing the consider parameters, $\boldsymbol{r}_k$ and $\dot{\boldsymbol{r}}_k$ are the inertial position and velocity respectively, c_D and c_R are the coefficients of drag and solar radiation pressure (SRP) respectively, T is the constant average thrust magnitude for the duration of the maneuver, and Δt_k is the constant satellite clock bias at time t_k. The consider parameters are the vector portion of the right handed attitude quaternion, $\boldsymbol{q}$, representing the rotation from the inertial frame to the body fixed frame (where $\bar{\boldsymbol{q}} = \begin{bmatrix} \boldsymbol{q}^T & q \end{bmatrix}^T$ is the full quaternion) and mass, m.

The state evolves according to the nonlinear reference trajectory dynamics[3]

$$\dot{\boldsymbol{x}}_k^* = f(\boldsymbol{x}_k^*, \boldsymbol{c}_k^*, t_k) \tag{5}$$

$$= \begin{bmatrix} \dot{\boldsymbol{r}}_k^{*T} & \ddot{\boldsymbol{r}}_k^{*T} & \mathbf{0}_{1\times(n-6)} \end{bmatrix}^T$$

$$\dot{\boldsymbol{\Phi}}(t_k, t_0) = \boldsymbol{F}_k \boldsymbol{\Phi}(t_k, t_0) \tag{6}$$

$$\dot{\boldsymbol{\theta}}(t_k, t_0) = \boldsymbol{F}_k \boldsymbol{\theta}(t_k, t_0) + \boldsymbol{B}_k \tag{7}$$

$$\boldsymbol{F}_k = \frac{\partial f(\boldsymbol{x}, \boldsymbol{c})}{\partial \boldsymbol{x}} \Big|_{\mathbf{x}=\mathbf{x}_k^*} \tag{8}$$

$$\boldsymbol{B}_k = \frac{\partial f(\boldsymbol{x}, \boldsymbol{c})}{\partial \boldsymbol{c}} \Big|_{\mathbf{x}=\mathbf{x}_k^*} \tag{9}$$

where $f(\cdot)$ represents the nonlinear nominal reference dynamics, $\ddot{\boldsymbol{r}}$ is the inertial acceleration, $\boldsymbol{F}_k$ and $\boldsymbol{B}_k$ are the state and consider dynamics Jacobians respectively, $\boldsymbol{\Phi}(t_k, t_0)$ is the state transition matrix from time t_0 to time t_k, and $\boldsymbol{\theta}(t_k, t_0)$ is the consider transition matrix from time t_0 to time t_k. The state and transition matrices are then propagated along the nominal trajectory from by the initial conditions: $\mathbf{x}_0^*$, $\boldsymbol{\Phi}(t_0, t_0) = \boldsymbol{I}$ and $\boldsymbol{\theta}(t_0, t_0) = \mathbf{0}$. The state and consider information can then be accumulated according to[3]

$$\boldsymbol{\Lambda}_{x,n} = \sum_{k=0}^{l} [\boldsymbol{H}_{x,k}\boldsymbol{\Phi}(t_k, t_0)]^T \boldsymbol{R}_k^{-1} [\boldsymbol{H}_{x,k}\boldsymbol{\Phi}(t_k, t_0)] \tag{10}$$

$$\boldsymbol{\Lambda}_{c,n} = \sum_{k=0}^{l} [\boldsymbol{H}_{x,k}\boldsymbol{\Phi}(t_k, t_0)]^T \boldsymbol{R}_k^{-1} \times \dots$$
$$[\boldsymbol{H}_{x,k}\boldsymbol{\theta}(t_k, t_0) + \boldsymbol{H}_{c,k}] \tag{11}$$

$$\boldsymbol{\lambda}_n = \sum_{k=0}^{l} [\boldsymbol{H}_{x,k}\boldsymbol{\Phi}(t_k, t_0)]^T \boldsymbol{R}_k^{-1} [h(\boldsymbol{x}_k^*, \boldsymbol{c}_k^*) - \boldsymbol{z}_k] \tag{12}$$

$$\boldsymbol{H}_{x,k} = \frac{\partial h(\boldsymbol{x}, \boldsymbol{c})}{\partial \boldsymbol{x}} \Big|_{\mathbf{x}=\mathbf{x}_k^*} \tag{13}$$

$$\boldsymbol{H}_{c,k} = \frac{\partial h(\boldsymbol{x}, \boldsymbol{c})}{\partial \boldsymbol{c}} \Big|_{\mathbf{x}=\mathbf{x}_k^*} \tag{14}$$

where $\boldsymbol{\Lambda}_{x,n}$ and $\boldsymbol{\Lambda}_{c,n}$ are the state and consider information matrices for iteration n, $\boldsymbol{\lambda}_n$ is the information state at iteration n, $h(\cdot)$ is the expected measurement given the nominal full state $\mathbf{x}_k^*$, $\boldsymbol{z}_k$ is the measurement vector, $\boldsymbol{R}_k$ is the measurement covariance matrix, and $\boldsymbol{H}_{x,k}$ and $\boldsymbol{H}_{c,k}$ represent the state and consider measurement sensitivities at t_k. With no *a priori* information about the state the information matrices are initialized to zero.

The accumulated information can then be used to determine the least-squares correction to the initial state, and the covariance in the initial state according to[3]

$$(\delta\hat{\boldsymbol{x}}_0)_n = \boldsymbol{\Lambda}_{x,n}^{-1}\boldsymbol{\lambda}_n \tag{15}$$

$$(\boldsymbol{P}_{xx,0})_n = \boldsymbol{\Lambda}_{x,n}^{-1} + \boldsymbol{S}_0\bar{\boldsymbol{P}}_{cc}\boldsymbol{S}_0^T \tag{16}$$

$$\boldsymbol{S}_0 = \boldsymbol{\Lambda}_{x,n}^{-1}\boldsymbol{\Lambda}_{c,n} \tag{17}$$

where $(\boldsymbol{P}_{xx,0})_n$ is the initial state covariance matrix corresponding to the nth filter iteration, and $\boldsymbol{S}_0$ is the initial consider sensitivity. Because the consider parameters are measured on-orbit, and thus, the corresponding sensor uncertainties are known *a priori* and assumed uncorrelated, they can be represented by the diagonal consider covariance matrix, $\bar{\boldsymbol{P}}_{cc}$. The filter is iterated until the correction to the initial state, $(\delta\hat{\boldsymbol{x}}_0)_n$, has converged. Assuming the error in the initial reference state is small and the measurement errors are small, this linearizion yields little error and the batch filter determines an acceptable solution.

State and Covariance Propagation

Assuming the reference dynamics of the system is representative of the true dynamics, the state and covariance can be propagated to find the nominal state and uncertainty for the orbital arc of interest. The initial state determined by the filter is propagated using the nonlinear reference dynamics given by Eq. (5). The initial state covariance, $\boldsymbol{P}_{xx,0}$, can be propagated to each measurement epoch using the accumulated state and consider transition matrices according to

$$\boldsymbol{P}_{xx,k} = \boldsymbol{\Phi}(t_k, t_0)\boldsymbol{P}_{xx,0}\boldsymbol{\Phi}(t_k, t_0)^T + \boldsymbol{S}_k\boldsymbol{P}_{cc}\boldsymbol{S}_k^T \quad (18)$$

$$\boldsymbol{S}_k = \boldsymbol{\Phi}(t_k, t_0)\boldsymbol{S}_0 + \boldsymbol{\theta}(t_k, t_0) \quad (19)$$

where the iteration subscript, n, is dropped but the equations hold true for any iteration's results. Equations (5,18-19) allow for a realization of the state and its uncertainty along the entire nominal trajectory. It is important to note, the batch filter framework only provides an estimate for an initial state, and thus, all dynamic states are referenced on the nominal trajectory and do not represent independent estimates of the state at time t_k.

MEASUREMENT MODELS

The thrust determination filter relies on both internal and external measurement processing. The internal measurements include the time stamp on all l pseudorange measurements, mass, and the attitude quaternion. These internal measurements are used in the propagation and accumulation of information but are not directly processed as part of the external measurement batch. The external measurements are then the series of L1/L2 GPS pseudoranges collected at all l measurement epochs. The pseudoranges are processed and then used to accumulate information in Equations (10-12). The models for all internal and external measurements are given in the following sections.

Time

For precise GPS navigation, an accurate realization of time is required. The satellite clock is modeled with a

constant random bias and white noise such that

$$\bar{t}_k = t_k + b_{t,k} + \nu_{t,k} \quad (20)$$

$$b_{t,k} = b_{t,k-1} + \epsilon_{b_t}(t_k - t_{k-1}) \quad (21)$$

where t_k is the true time of an observation, $\bar{t}_k$ is the time stamp for the observation, $b_{t,k}$ and $\nu_{t,k}$ are the clock bias and noise parameters respectively, and ϵ_{b_t} is the clock bias instability. However, the filter state estimates a constant time bias for each measurement epoch according to

$$t_k = \bar{t}_k + \Delta t_k \quad (22)$$

$$\Delta t_k = -b_{t,k} - \nu_{t,k} \quad (23)$$

where Δt_k is the constant time bias for time t_k in the state vector. The time biases are estimated independently at each measurement epoch to avoid errors from inaccurate clock modeling. The biases found in the initial state vector from the previous iteration of the filter are then used to update the nominal time stamps for the measurement batch such that

$$(t_k^*)_{n+1} = \bar{t}_k + (\Delta t_k)_n \quad (24)$$

The updated realization of time is used to propagate the state, generate more accurate expected measurements, and re-interpolate the GPS ephemerides.

Attitude

Attitude is the second internal measurement in the filter scheme. The attitude is used to account for the location of the GNSS receiver onboard APEX, define the thrust vector, and determine relative cross sectional areas in the drag and SRP dynamics. Errors in the attitude quaternion returned by the APEX star tracker are modeled as a small angle deviation[4] composed of a constant random bias and white noise parameter such that

$$\Delta\boldsymbol{\theta}_k = \boldsymbol{b}_{str,k} + \boldsymbol{\nu}_{str,k} \quad (25)$$

$$\bar{\boldsymbol{q}}_{m,k} = \begin{bmatrix} \frac{1}{2}\Delta\boldsymbol{\theta}_k \\ 1 \end{bmatrix} \otimes \bar{\boldsymbol{q}}_k \quad (26)$$

where $\Delta\boldsymbol{\theta}_k$ is the small angle deviation, $\boldsymbol{b}_{str,k}$ and $\boldsymbol{\nu}_{str,k}$ are the star tracker bias and noise parameters, $\bar{\boldsymbol{q}}_{m,k}$ and $\bar{\boldsymbol{q}}_k$ are the measured and true attitude quaternions respectively. The $\otimes$ operator indicates quaternion multiplication.

However, attitude measurements may be recorded at a higher frequency than pseudoranges or may not properly align with measurement epochs as desired. In light of this, a quaternion interpolation scheme must also be implemented to allow for flexible dynamics propagation and measurement processing. To improve interpolation within the quaternion unit norm constraint, a Spherical Linear Quaternion Interpolation (SLERP)[5] method is employed. For a desired attitude state at time t_k that

lies between the measured quaternions at times $\bar{t}_i$ and $\bar{t}_j$ (where $\bar{t}_i < \bar{t}_j$), the interpolated quaternion, $\bar{q}_{m,k}$, is given by

$$\bar{q}_{m,k} = \frac{\bar{q}_{m,i} sin((1-\tau)\Omega) + \bar{q}_{m,j} sin(\tau\Omega)}{sin(\Omega)} \quad (27)$$

$$\tau = \frac{t_k - t_i}{t_j - t_i} \quad (28)$$

$$\Omega = cos^{-1}(\bar{q}_{m,i} \cdot \bar{q}_{m,j}). \quad (29)$$

It can be seen that Eq. (27) is undefined for the case where $\bar{q}_{m,i} = \pm\bar{q}_{m,j}$. To maintain numerical stability, a Linear Quaternion Interpolation (LERP)[5] method is employed where $||\bar{q}_0 \cdot \bar{q}_1|| > 0.9995$ such that

$$\bar{q}_{m,k} = \bar{q}_{m,i}(1-\tau) + \bar{q}_{m,j}\tau. \quad (30)$$

GPS Pseudorange

Dual frequency L1 and L2 pseudoranges from the GPS constellation are the external measurements. A common pseudorange model for either frequency is given by[3]

$$p_{s,k} = ||\boldsymbol{\rho}_{s/rx,k}|| + c(\Delta t_k^{APEX} - \Delta t_k^s) + \phi_k + \nu_{GPS,k} \quad (31)$$

$$\boldsymbol{\rho}_{s/rx,k} = \boldsymbol{r}_k^i + \boldsymbol{T}_i^b(\bar{q}_{m,k})^T \boldsymbol{r}_{rx}^b - \boldsymbol{r}_{s,k}^i + \boldsymbol{T}_{b,s}^i \boldsymbol{r}_{pc,s}^b \quad (32)$$

where $p_{s,k}$ is the pseudorange generated from GPS satellite s, Δt_k^{APEX} is the GNSS receiver clock bias that is estimated in the initial state, Δt_k^s is the clock bias of GPS satellite s, c is the vacuum speed of light, $\phi_{s,k}$ is the ionospheric delay, and $\nu_{GPS,k}$ is the receiver white noise. The geometric range is given by the Euclidean norm ($|| \cdot ||$) of the vector between the phase center of the GPS transmitter and GNSS receiver phase center, $\boldsymbol{\rho}_{s/rx,k}$, given by Eq. (32), where $\boldsymbol{r}_k^i$ is the inertial position of APEX, $\boldsymbol{T}_i^b(\bar{q}_{m,k})$ is the rotation from the inertial frame to the APEX body frame given the reference attitude quaternion, $\boldsymbol{r}_{rx}^b$ is the location of the GNSS receiver phase center in the body frame, $\boldsymbol{r}_{s,k}^i$ is the inertial position of the center of mass of GPS satellite s, $\boldsymbol{T}_{b,s}^i$ is the known rotation from the GPS body frame to the inertial frame, and $\boldsymbol{r}_{pc,s}^b$ is the location of the phase center in the GPS body frame. This model can be used interchangeably between L1 and L2 pseudoranges provided the correct phase center and ionospheric correction for the specific frequency are implemented correctly. To remove a vast majority of the ionospheric error in L1/L2 pseudorange pairs, a first order correction can be utilized such that[3]

$$\tilde{p}_{s,k} = \gamma_1 p_{s_1,k} - \gamma_2 p_{s_2,k} \quad (33)$$

$$\gamma_1 = \frac{f_1^2}{f_1^2 - f_2^2} \quad (34)$$

$$\gamma_2 = \frac{f_2^2}{f_1^2 - f_2^2} \quad (35)$$

where $\tilde{p}_{s,k}$ is the equivalent pseudorange corrected for ionospheric effects, γ_1 and γ_2 are scaling terms, and f_1 and f_2 are the frequencies for L1 and L2 respectively (1,575.42 MHz for L1 and 1,227.60 MHz for L2). This correction method is applied to all pseudorange measurement pairs at a given measurement epoch. It is important to note that combining dual frequency pseudoranges generates a new range with respect to an intermediate phase center not located at either the L1 or L2 transmission phase centers. To avoid errors from difficult to predict ionospheric interference and the equivalent phase center, the expected measurement is produced by evaluating Eq. (31) for the L1 phase center without the ionospheric or white noise terms. For GPS satellites, the L1 and L2 phase centers are relatively co-located[6] and as such, this assumption will usually only introduce millimeter or sub-millimeter level errors. The measurement noise covariance must also be corrected for the combination of dual frequency measurements. The two white noise parameters are assumed uncorrelated and, as such, have an increased measurement covariance given by

$$\sigma_{\tilde{p}}^2 = \sigma_p^2(\gamma_1^2 + \gamma_2^2) \quad (36)$$

where $\sigma_{\tilde{p}}^2$ is the equivalent pseudorange covariance and σ_p^2 is the covariance for the receiver white noise present and independent for both L1 and L2 pseudoranges.

The relevant measurement partials are then given by

$$\frac{\partial \tilde{p}_s}{\partial \boldsymbol{r}}\Big|_{\mathbf{x}=\mathbf{x}_k^*} \approx \frac{\boldsymbol{\rho}_{s_1/rx,k}^T}{||\boldsymbol{\rho}_{s_1/rx,k}||} \quad (37)$$

$$\frac{\partial \tilde{p}_s}{\partial \Delta t_k}\Big|_{t=t_k^*} = c \quad (38)$$

$$\frac{\partial \tilde{p}_s}{\partial \boldsymbol{q}}\Big|_{\mathbf{x}=\mathbf{x}_k^*} \approx \frac{-\partial \tilde{p}_s}{\partial \boldsymbol{r}}\Big|_{\mathbf{x}=\mathbf{x}_k^*} \left[\boldsymbol{T}_i^b(\bar{q}_{m,k})^T \boldsymbol{r}_{rx}^b \times \right] \quad (39)$$

where the partial is taken assuming the equivalent phase center can be approximated at the L1 phase center and evaluated at the nominal position and measurement time, $\left[\boldsymbol{a} \times \right]$ is the skew symmetric matrix, and where the derivative of the equivalent pseudorange with respect to the vector portion of a quaternion is approximated by linearizing the multiplicative residual about the nominal state.[4] All measurement partials not shown are taken to be zero.

To improve accuracy of GPS position and timing beyond the broadcast ephemeris, the International GNSS Services (IGS) Final Data Product,[6] which contain posterior fits for the position and clock states of each satellite in the GPS constellation, was used. The data are published in fifteen minute intervals for the GPS day of interest. To determine the position and clock bias at the epoch of interest, a standard Lagrange Interpolation scheme was

utilized.[1,7] The L1 and L2 phase center locations with respect to the GPS satellite's center of mass are also published by IGS in the body-fixed frame for the satellite of interest. The rotation from the body-fixed frame to in inertial frame is found by approximating the attitude of the GPS satellite. The body z axis is assumed nadir pointing, the body y axis points in the direction of the cross product of the body z vector and the vector from the satellite's center of mass to the Sun, and the body x axis completes the orthogonal triad.[6] The resulting combination of both data products provides an accurate approximation of the broadcast phase center for determining the expected pseudoranges in Equations (31-32). It is also important to note that all GPS position and clock parameters should be determined at the broadcast epoch not the at the time of reception.[1] This is accomplished given a realization of the measurement time and the nominal state by determining the time of transmission such that

$$c(t_k^* - t_{tx,s}) = \boldsymbol{\rho}_{s/rx,k}(t_{tx,s}, \mathbf{x}_k^*) \qquad (40)$$

is true, where $t_{tx,s}$ is the time of transmission from GPS satellite s, and the geometric range is determined from the reference state and the GPS parameters interpolated at time $t_{tx,s}$.

Measurement Vector and Covariances

The external measurement vector, $\boldsymbol{z}$, is then the series of m equivalent pseudoranges found by evaluating Eq. (33) for all m L1/L2 pseudorange pairs at time t_k such that

$$\boldsymbol{z}_k = \begin{bmatrix} \tilde{p}_{1,k} & \tilde{p}_{2,k} & \dots & \tilde{p}_{m,k} \end{bmatrix}^T. \qquad (41)$$

The covariance matrix at t_k, $\boldsymbol{R}_k$, is then the $m \times m$ diagonal matrix with entries on the main diagonal all equal to Eq. (36) for a given receiver noise covariance. The consider states are assumed uncorrelated and the covariance matrix, $\bar{\boldsymbol{P}}_{cc}$, is given by a diagonal matrix whose entries are the *a priori* covariances for the elements $\Delta\boldsymbol{\theta}$ and mass for the state order shown in Eq. (4) and are determined by the flight sensors.

The full proposed filter algorithm, composed of the batch filter architecture presented in conjunction with the above measurement models, is provided in the Appendix. The presented framework and measurement models need not be the only states or observations. The filter framework is highly adaptable to additional states, observations and/or dynamics models. The inclusion of the IGS precise GPS data products, allows for vastly improved position estimates which, in general, significantly aids in the estimation of other states and is easily adapted to improve numerous other CubeSat missions.

STK VERIFICATION

To determine the statistical consistency of the proposed filter design a 1,000 trial Monte Carlo analysis was conducted. To remain computationally tractable, and to align with further verification, a single true trajectory was generated using Analytic Graphic Inc. Systems Took Kit (STK) software. The true trajectory was determined using EGM2008 gravity data with a one hundred degree and order spherical harmonics model, fourth degree and order ocean tide effects, spherical drag with a constant cross sectional area, a Jaccia-Roberts atmospheric density model, spherical solar radiation pressure with a constant cross sectional area, and n-body perturbations from the Jupiter and Saturn systems, Sun, Moon, Mars, and Venus. The true position and time states of all satellites in the GPS constellation were resampled from the interpolated statistics found in the IGS data products for each trial. The initial timing, orbit, and maneuver parameters are displayed in Tables 1-2.

Table 1: Simulation Timing Parameters

Parameter	Value	Units/Frame
Date	July 19 2010	UTC
t_0	9:59:45.000	UTC
Initial Maneuver Epoch	11:29:45.000	UTC
Burn Duration	1500	s
t_f	13:24:45.000	UTC

Table 2: True Initial Orbit and Vehicle Parameters

Parameter	Value	Units/Frame
Semimajor Axis	6923.32	km
Eccentricity	4.18413×10^{-3}	
Inclination	94.0515	deg
RAAN	128.232	deg
Arg. of Perigee	244.409	deg
True Anomaly	346.030	deg
Static Attitude	$\bar{q} = \begin{bmatrix} -0.330135 \\ -0.0795817 \\ 0.320042 \\ 0.884450 \end{bmatrix}$	J2000 to Body-Fixed
c_D	2.2	
c_R	1.0	
Thrust	33	μN

A single static attitude quaternion was used for truth to remain tractable for numerous Monte Carlo trials. This quaternion places the thrust vector, pointed along the positive body x direction, in approximately the positive orbit angular momentum direction. This orientation was

found to best separate the effects of drag and thrust and improve filter performance.[1] Additionally, the effects of attitude control are beyond the scope of this work and were neglected, however, the filter framework is capable of functioning using high frequency discrete attitude measurements for a dynamic attitude state and covariance associated with any off-nominal attitude motion (such as unexpected thrust torques) or control. An equal number of measurements were processed before and after the maneuver to improve performance.

For each trial the internal and external sensor noise and bias terms are modeled as Gaussian distributions with standard deviations shown in Table 3. The initial state guess, $(\boldsymbol{x}_0^*)_0$, used to seed the filter for each trial was also taken to be Gaussian with the true initial state as the mean and standard deviation shown in Table 3. The time bias states in the initial state guess were all initialized to zero.

Table 3: Monte Carlo Simulation Statistics

Parameters	Distribution 1σ	Units
Clock noise	2.0	μs
Initial clock bias	10	μs
Clock bias instability	10	ns/s
Star tracker bias	1	deg
Star tracker noise	0.0025	deg
Mass bias	100	g
Pseudorange Noise	0.1	m
Initial position	100	m
Initial velocity	1.0	m/s
c_D	0.1	
c_R	0.1	
Thrust	1.0	mN

The filter dynamics model includes seventy two degree and order nonspherical effects[8] using EGM2008 gravity data,[9] a spherical drag and solar radiation pressure force model with variable cross sectional area determined by the attitude of the spacecraft,[4] an exponential atmospheric model,[8] and Sun and Moon perturbations.[8] For tractability, only ten degree and order gravity harmonics were used in the calculation of the dynamics Jacobian entries relating to gravitational acceleration. All other dynamics parameters are neglected by the filter for this verification. The state and transition matrices are propagated to each realized measurement epoch, t_k^*. For simplicity, only L1 pseudoranges were considered and ionospheric effects were neglected in both measurement simulation and filtering. This was done to avoid difficult ionospheric modeling while still verifying equivalent pseudorange measurement processing within the proposed filter framework. The position and clock states

of each GPS satellite were taken as the mean value interpolated from IGS ephemeris. The measurement covariance matrix's main diagonal was populated by the covariance of the pseudorange noise parameter in Table 3. Because the attitude quaternion is static for each trial, the consider covariance matrix is also static, with the diagonal elements relating to attitude equal to the addition of the star tracker bias and noise covariances. For the purposes of this simulation, the star tracker bias will simulate standard biases (such as camera misalignment etc.) and thrust vector misalignment.

The initial position from each filter solution was propagated along the nominal trajectory and the error between the true and nominal trajectories were calculated. The position error statistics are shown in Figure 2. The errors from a single filter trial is shown in red (—) and accompanying $\pm 3\sigma$ intervals for the same trial were extracted from the main diagonal of the covariance matrix at each measurement epoch and are shown as a solid black line (—). The standard deviation of the position errors from all 1,000 Monte Carlo trials was determined and the $\pm 3\sigma$ data were plotted as a dashed gray line (- -). Figure 3 displays the average nominal velocity errors from each trial as a solid gray line (—).

The filter was able to determine the position of the satellite with half-meter level accuracy (3σ) for the entirety of the simulation with centimeter level accuracy (3σ) for a majority of the simulated trajectory along all three axes. The single trial error is well contained in the filter's determined $\pm 3\sigma$ interval for the majority of the trajectory. Of interest for filter verification is the slight underestimation of the standard deviations in the position states. This is most likely due to gravity model mismatch and reduced gravity gradient order in the dynamics Jacobian calculation. For individual filter runs, such as that expected from APEX flight data, errors in the gravity model can be mitigated as the run-time requirement is substantially relaxed. For the parameters neglected to improve Monte Carlo simulation run-time, the position solutions are reasonably accurate and are well within the requirements of the APEX mission.

Of particular importance to the APEX mission is the thrust estimation. To meet the mission requirements, the filter must achieve a thrust accuracy lower than 10% (1σ) of the nominal thrust value. For the nominal electric mode performance simulated, the filter must determine thrust within 3.3 μN (1σ) in addition to any additional biases produced by differences in dynamics and linearization errors. The distribution of all 1,000 thrust errors were plotted as a histogram in Fig. 4 with the mean error displayed as a solid vertical black line (—) and the $\pm 3\sigma$ interval determined by a single trial shown as vertical dashed black lines (- -). The mean thrust error
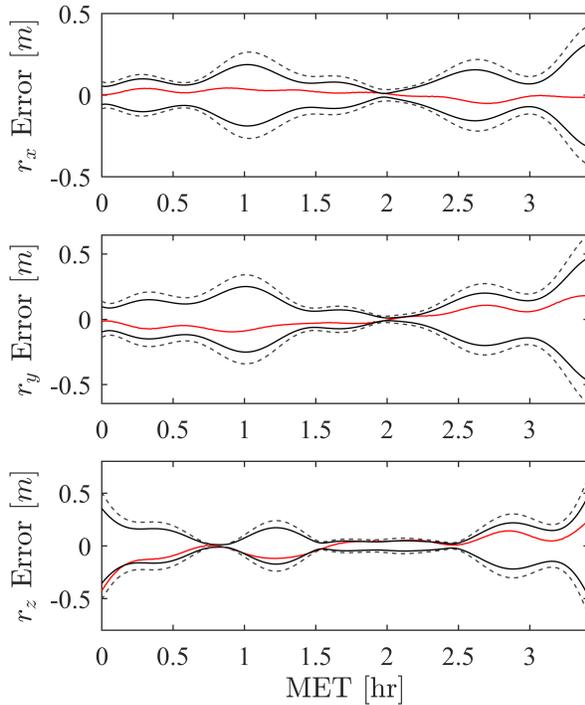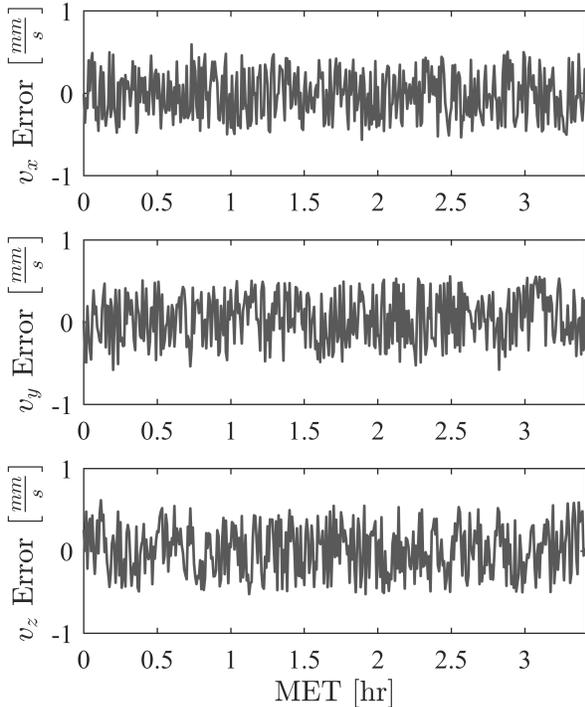
Figure 2: Nominal Position Error Statistics

Figure 3: Mean Velocity Errors

of all 1,000 trials was found to be 0.84547 μN, which represents approximately 2.6% of the nominal thrust. The nonzero mean is attributed to both the reduced gravity model order and inaccuracy in the reduced filter dynamics. This bias can be mitigated for single runs, but, in general is well contained within the mission requirements. Moreover, the average standard deviation of the thrust estimate returned by the filter was 0.34453 μN, or approximately 1% of the nominal true thrust and almost ten times less than the mission requirement. The determined standard deviation was an underestimate of the Monte Carlo standard deviation by 0.06125 μN, and, as shown in Fig. 4, contains the vast majority of all Monte Carlo errors. Both the error bias and distribution statistics combined are well below the 10% error requirement (1σ) for the APEX mission. Even more promising is the margin represented by the thrust error statistics, with both the bias and 3σ confidence interval together below the 10% error requirement.
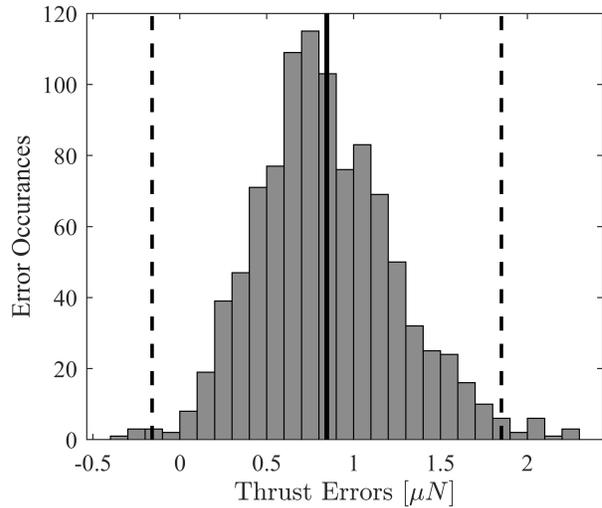

Figure 4: Thrust Error Statistics

INITIAL ICESAT VERIFICATION

With the statistical consistency of the filter verified, the next step becomes testing the robustness and accuracy of the algorithm with real mission data. The NASA Ice, Cloud, and Elevation (ICESat) mission was chosen for flight data verification due to the documentation, accessibility, and trove of pseudorange and attitude data. The primary purpose of the NASA ICESat mission was the determination of inter-annual and long-term changes in polar ice-sheet volume to sufficient accuracy to assess their impact on global sea level.[10] To accomplish this task, the position of the Geoscience Laser Altimeter System (GLAS) reference point in space, as well as the

pointing direction of the GLAS, must be accurately determined through processes referred to as Precision Orbit Determination (POD) and Precision Attitude Determination (PAD) respectively. The GPS-derived POD used for the ICESat mission employs the measurements from one JPL BlackJack receiver/antenna combinations along with data products provided by the International GNSS Service and the International Earth Rotation Service[11] and has been verified to produce position estimates with a radial accuracy to within 1-2 cm.[12] The PAD methodology used for the ICESat mission is based on the application of the Extended Kalman Filter to Instrument Star Tracker (IST), Laser Reference Sensor (LRS), and gyroscope measurements.[13] ICESat PAD has been verified to produce attitude estimates with 2 arcsec (1σ) accuracy,[12] although publicly available data are reported only to have an attitude estimation error less than 10 arcsec. ICESat publicly available GPS measurements, position, and attitude solutions are thus, ideal for verification of the APEX thrust determination filter using real mission data.

To verify the performance of the APEX thrust determination filter using ICESat data, a batch of L1 and L2 GPS pseudorange measurements were processed by the filter while employing interpolated PAD solutions to propagate the state and to generate expected pseudorange measurements. For the period evaluated, ICESat did not conduct active thrusting, thus, for the filter to perform properly, it must converge to a thrust estimate of approximately zero. With a null true thrust, the resulting thrust estimate will also provide insight into the sensitivity of the filter with flight data. To align with the STK verification and the anticipated maneuver for APEX, the thrust vector was defined along the $\hat{y}$-direction of the ICESat body frame, nearly perpendicular to the velocity of the spacecraft, with a null true magnitude. The resultant state estimate was then compared to the published POD solution as near truth. Table 2 displays the epoch corresponding to the initial reference state and initial measurement, which aligns with the initial reference trajectory used for STK verification. ICESat data were evaluated over a one hour arc with the maneuver lasting 3000 s, starting at 10:08:45.000 UTC. Table 2 displays the initial, near truth, orbit state within the published ICESat POD solutions.

Table 4 displays the estimation error of the initial reference state and thrust magnitude. The dynamic states of ICESat were estimated within a reasonable accuracy for the first iteration, although, the estimates lie outside the desired accuracy for the filter design. The effects due to a laterally varying atmospheric density and rotating solar panels on ICESat are neglected within the filter's dynamic model, and are the likely causes, among others, for the estimation error that is seen. These po-

tential error sources will be mitigated on smaller CubeSat form-factors with substantially lower complexity in the dynamics. Thus, improved accuracy is expected for the estimation of the APEX position and velocity respectively. Additionally, delays in GPS pseudo-random noise propagation due to the ionosphere, though easy to correct in the measurements, are more difficult to correct when determining an accurate time of transmission necessary for generating expected measurements. The delay is a function of the length of time the wave must travel through and the density of the ionosphere. This is the most likely contributor to meter-level errors in the processing of expected pseudoranges. Future work will focus on improving ionospheric modeling.

Table 4: Estimation Errors

Error Parameter	Value	Units
r_x	3.8978	m
r_y	-33.0145	m
r_z	0.2937	m
v_x	-0.0983	m/s
v_y	0.0835	m/s
v_z	-0.1004	m/s
Thrust	1.0985	mN

The thrust over the course of a 3000 s evaluation arc was determined to within millinewton level accuracy. This resolution, though higher than the APEX mission thrust, is a promising first step in verification of the filter when the drastic mass differences between APEX and ICESat are taken into account. The ICESat mission at the epochs processed, had a mass of 882 kg. Thus, the determined millinewton error represent errors on the order of ten micronewtons if the equivalent acceleration is applied to a 10 kg 6U CubeSat. Though this error is outside the 3.3 μN (1σ) error margin, improvements to atmospheric modeling and drastic reductions in dynamical complexity present with CubeSats is expected to allow for sub-meter position errors and micronewton thrust accuracy in the final filter design.

CONCLUSION

An improved consider batch filter was developed to ingest GPS and star tracker data and determine a precise thrust estimate for the experimental MIME thruster payload onboard the APEX CubeSat. In addition to thrust, it was also capable of accurate position determination along the nominal reference trajectory. The filter framework is also easily extended to future M-SAT and other small satellite missions, and allows for accurate position estimates, along with other potentially desired parameters, from commonly flown CubeSat sensors. The sta-

tistical consistency and dynamics model of the batch filter were verified from a 1,000 trial Monte Carlo analysis with a high fidelity true trajectory simulated using AGI's STK software. The filter was shown to determine unbiased position solutions with primarily centimeter-level accuracy throughout the reference orbits. The Monte Carlo also verified that both the bias and distribution of the thrust errors were well within the mission requirements for APEX. An initial investigation into flight data performance was presented using the NASA ICESat-1 mission dual frequency pseudorange measurements and precise orbit determination values. Given the more complicated dynamics of ICESat and the current state of the atmospheric models, the filter performed reasonably well. The filter demonstrated sensitivity to accelerations at a near equivalent order of magnitude as APEX while operating with a less than desirable expected pseudorange model.

Future work will focus on improved determination of the true time of transmission of GPS satellites necessary for high accuracy position and thrust determination. It is expected that with slight improvements to measurement processing, ICESat thrust and position estimates can be determined by the current framework within the APEX mission requirements.
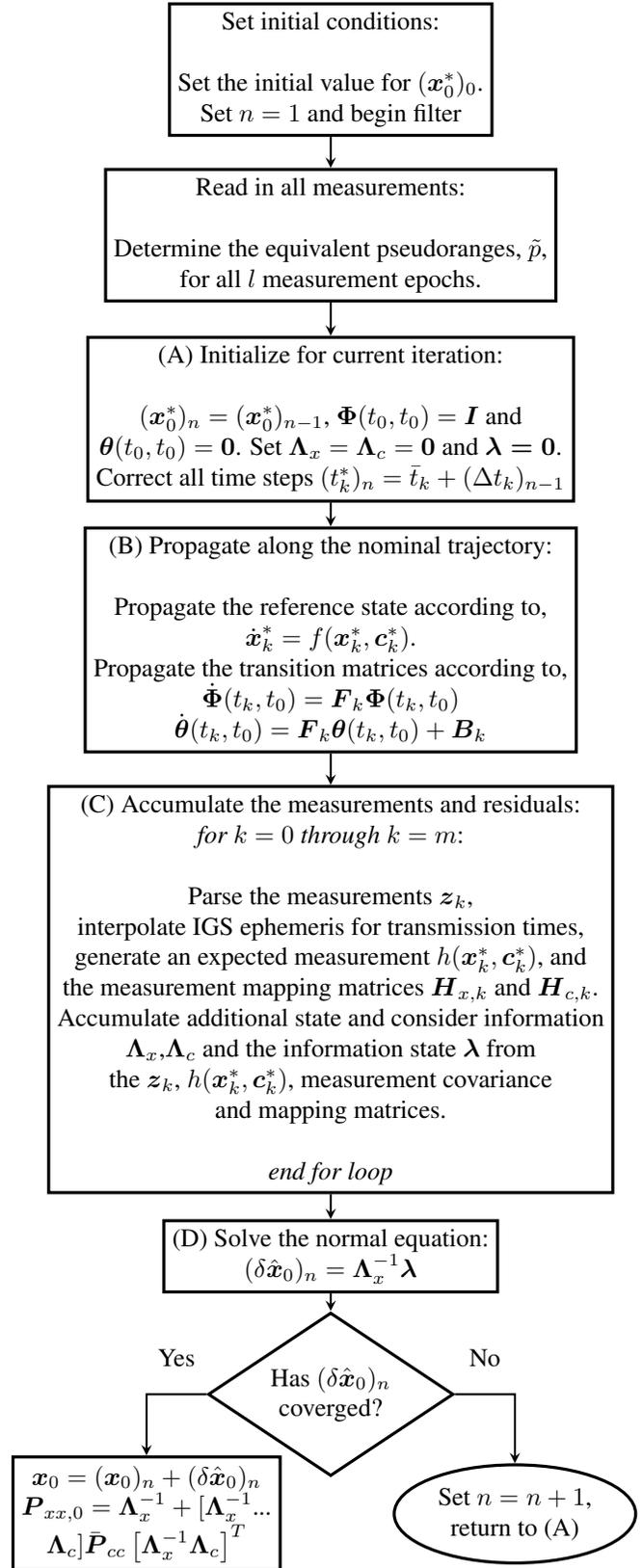
APPENDIX: FILTER ALGORITHM DIAGRAM

Set initial conditions:

Set the initial value for $(\boldsymbol{x}_0^*)_0$.
Set $n = 1$ and begin filter

Read in all measurements:

Determine the equivalent pseudoranges, $\tilde{p}$, for all l measurement epochs.

(A) Initialize for current iteration:

$(\boldsymbol{x}_0^*)_n = (\boldsymbol{x}_0^*)_{n-1}$, $\boldsymbol{\Phi}(t_0, t_0) = \boldsymbol{I}$ and $\boldsymbol{\theta}(t_0, t_0) = \boldsymbol{0}$. Set $\boldsymbol{\Lambda}_x = \boldsymbol{\Lambda}_c = \boldsymbol{0}$ and $\boldsymbol{\lambda} = \boldsymbol{0}$.
Correct all time steps $(t_k^*)_n = \bar{t}_k + (\Delta t_k)_{n-1}$

(B) Propagate along the nominal trajectory:

Propagate the reference state according to,
$\dot{\boldsymbol{x}}_k^* = f(\boldsymbol{x}_k^*, \boldsymbol{c}_k^*)$.
Propagate the transition matrices according to,
$\dot{\boldsymbol{\Phi}}(t_k, t_0) = \boldsymbol{F}_k \boldsymbol{\Phi}(t_k, t_0)$
$\dot{\boldsymbol{\theta}}(t_k, t_0) = \boldsymbol{F}_k \boldsymbol{\theta}(t_k, t_0) + \boldsymbol{B}_k$

(C) Accumulate the measurements and residuals:
for $k = 0$ through $k = m$:

Parse the measurements $\boldsymbol{z}_k$,
interpolate IGS ephemeris for transmission times,
generate an expected measurement $h(\boldsymbol{x}_k^*, \boldsymbol{c}_k^*)$, and
the measurement mapping matrices $\boldsymbol{H}_{x,k}$ and $\boldsymbol{H}_{c,k}$.
Accumulate additional state and consider information
$\boldsymbol{\Lambda}_x, \boldsymbol{\Lambda}_c$ and the information state $\boldsymbol{\lambda}$ from
the $\boldsymbol{z}_k$, $h(\boldsymbol{x}_k^*, \boldsymbol{c}_k^*)$, measurement covariance
and mapping matrices.

end for loop

(D) Solve the normal equation:
$(\delta\hat{\boldsymbol{x}}_0)_n = \boldsymbol{\Lambda}_x^{-1} \boldsymbol{\lambda}$

Yes   Has $(\delta\hat{\boldsymbol{x}}_0)_n$ coverged?   No

$\boldsymbol{x}_0 = (\boldsymbol{x}_0)_n + (\delta\hat{\boldsymbol{x}}_0)_n$
$\boldsymbol{P}_{xx,0} = \boldsymbol{\Lambda}_x^{-1} + [\boldsymbol{\Lambda}_x^{-1} ...$
$\boldsymbol{\Lambda}_c] \bar{\boldsymbol{P}}_{cc} \left[\boldsymbol{\Lambda}_x^{-1} \boldsymbol{\Lambda}_c\right]^T$

Set $n = n + 1$, return to (A)

Figure 5: Filter Design Diagram

REFERENCES

1. K. J. Craft, J. E. Darling, and H. J. Pernicka, "Performance Determination of a Multi-Mode Thruster Using GPS and Star Tracker Data," *Proceedings of the 41st Annual IEEE Aerospace Conference*, Big Sky, MT, March 2020.

2. B. W. Morton, "Quantifying On-Orbit Performance of CubeSat Micropropulsion Systems by Observing Orbital Element Variations," M.S. Thesis, Missouri Univ. of Science and Technology, Rolla, MO, May, 2018.

3. B. D. Tapely, B. E. Schutz, and G. H. Born, *Statistical Orbit Determination*. Elsevier Inc., 2004.

4. F. L. Markley and J. L. Crassidis, *Fundamentals of Spacecraft Attitude Determination and Control*. Springer, New York, 2014.

5. E. Dam, M. Koch, and M. Lillholm, *Quaternions, Interpolation and Animation*. Rapport (Københavns universitet. Datalogisk institut), Datalogisk Institut, Københavns Universitet, 1998.

6. G. Johnston, A. Riddel, and G. Hausler, *The International GNSS Service. In Teunissen, Peter J.G., Montenbruck, O. (Eds.), Springer Handbook of Global Navigation Satellite Systems*. Cham, Switzerland: Springer International Publishing, pp. 967-982, 2017.

7. Y. Feng and Y. Zheng, "Efficient Interpolations to GPS Orbits for Precise Wide Area Applications," *GPS Solut: Springer-Verlag*, 2005.

8. D. A. Vallado and W. D. McClain, *Fundamentals of Astrodynamics and Applications*. Microcosm Press, Hawthorne, CA, 2013.

9. N. K. Pavlis, S. A. Holmes, S. C. Kenyon, and J. K. Factor, "The Development and Evaluation of the Earth Gravitational Model 2008 (EGM2008)," *Journal of Geophysical Research: Solid Earth (1978 - 2012)*, vol. 117, 2012.

10. H. Zwally and et. al., "ICESat's Laser Measurements of Polar Ice, Atmosphere, Ocean, and Land," *Journal of Geodynamics*, vol. 34, no. 3, pp. 405 – 445, 2002.

11. B. E. Schutz, H. J. Zwally, C. A. Shuman, D. Hancock, and J. P. DiMarzio, "Overview of the ICESat Mission," *Geophysical Research Letters*, vol. 32, p. L21S01, Nov. 2005.

12. B. Schutz, S. Bae, N. Smith, and M. Sirota, ""Precision Orbit and Attitude Determination for ICESat"," *Advances in the Astronautical Sciences*, vol. 132, 01 2008.

13. H. J. Rim and B. E. Schutz, "Precision Orbit Determination (POD)," Oct 2002.